International Journal for Housing Science and Its Applications
Publish August 6, 2025. Volume 46, Issue 3 Pages 5404-5411

https://doi.org/10.70517/ijhsa463466

Research on the Application of Digital Modeling Technology in Visual Communication Design for Artistic Expression and Technological Innovation

Dongyun Lin[1,*]
[1] Guangzhou College of Technology and Business, Guangzhou, Guangdong, 510000, China
Corresponding authors: (e-mail: lindongyun2025@163.com).

Abstract The increasing development and maturity of digital modeling technology makes its application integration in visual communication design possible. This paper proposes a multi-visual 3D animation modeling method by combining visual communication design and digital modeling technology. For the difficulty of drawing curved objects in the modeling process, a luminance interpolation method is used to deal with the surface of objects represented by arbitrary raised polygons. At the same time, Virtools interactive software is used for the design and production of 3D interactive animation. In addition, based on the experimental results, the improved SIFT algorithm with higher matching accuracy and shorter matching time is chosen as the image feature extraction algorithm. By integrating dynamic interaction and modeling, the innovative performance and application of digital modeling technology in visual communication design is realized. In the overall performance of the proposed technology, the difference between the expected and tested values of several indexes is controlled in the interval of [-5,5], which has a high degree of matching with the expected user experience.

Index Terms visual communication design, improved SIFT algorithm, digital modeling, 3D interactive animation

I. Introduction

In the context of the rapid development of digital media advertising, three-dimensional animation design and other fields, visual communication design occupies an important position in the process of modern art design [1]. Visual communication is a kind of communication between human beings using visual viewing form, which is a way of expression and dissemination through visual language [2]. It contains the concepts of both visual symbols and communication, by setting visual symbols in the image and communicating them to the viewer through the designer's thoughts, so that the viewer becomes the audience of the designer's thoughts [3], [4].

With the arrival of the digital era and the continuous improvement of digital imaging technology, three-dimensional images have been playing a great auxiliary role in the development of visual communication technology. The mutual integration of digital media advertising and three-dimensional modeling technology to express the intention of product design can not only highlight the function of the product, but also show the special significance of product creation [5]-[7]. Compared with two-dimensional graphic design, three-dimensional design is indeed richer in terms of expression, for example, in terms of conveying the effect of the extreme can attract a lot of people's attention, and at the same time, three-dimensional conveying design is more three-dimensional, so it can be more full of the designer's thoughts in the creation of the design [8]-[11]. In the whole process of visual communication, the interpretation of information and the reception of visual symbols is a complicated process [12]. Therefore, designers or engineers need to use highly skilled and capable graphic design tools to realize engineering or product design, so that the visual communication design has the initiative and positivity of communication [13], [14].

This paper elaborates the 3D animation modeling methods and steps based on visual communication design system as the overall application method of digital modeling technology in visual communication design. Then, in view of the drawing problem of curved objects in modeling, the paper explains the solution process and drawing method of Gourand luminance interpolation method and Phong normal vector interpolation method for a variety of curved objects. Briefly analyze the overall functions and application framework of Virtools interactive software, and use the software to create 3D interactive animation. Then we design the comparison experiment of SIFT algorithm before and after the improvement, and select the appropriate algorithm configuration. We also take the corridor bridge space as the experimental object to compare the 3D modeling efficiency of the proposed method with

similar methods. Finally, the non-functional module test, the overall functional test and the dynamic interactive display sensitivity verification of the system based on the method of this paper are carried out sequentially.

II. 3D modeling technology based on visual communication design

II. A.Multi-visual 3D animation modeling

Multi-visual 3D animation model construction is based on the modeling and scene design in the pre-design stage, generating a depth judgment model in the variational mode based on the image sequence at the key frames of multi-visual animation, obtaining the original depth map of the animation with reference to the principle of discrete-space sampling, optimizing the depth model of the animation image through the initial pairwise principle, and solving the multi-visual 3D animation model based on this judgment.

The $A\left(\frac{|w_{ji}|}{\alpha_{ji}},\alpha_T\right)$ and Q_i are used to describe the objective function of the camera's position judgment and the sampling region of the initialized map of the animated image obtained from the styling and scenography in the pre-design phase, respectively, where w_{ji} and α_{ji} describe the projection error and the unbiased estimation of the standard deviation of feature point matching in the i th key frame of the animation image, respectively.

The initialized map is co-completed with reference to the overall LM cluster correction principle, and the formula is described as equation (1):

$$\left\{\left(\tau_1,\tau_2,\ldots,\tau_N\right)\left\{y_1,y_2,\ldots,y_M\right\}\right\}=\arg\min\sum_{i=1}^{N}\sum_{j\in Q_i}A\left(\frac{\left|w_{ji}\right|}{\alpha_{ji}},\alpha_T\right) \tag{1}$$

where, τ_i and y_i describe the camera position hexadecimal description vector of the i th keyframe of the animation image and the 3D feature points of the generated scene, respectively.

Assuming that the multivision animated image has light fixity and depth map smoothness, Eq. (2) can describe the animated image depth energy function model:

$$W_d=\int_{\psi}\left(W_{da}y_i+\delta W_{re}\right)d\varepsilon \tag{2}$$

where, W_{da} and W_{re} describe the animated image data penalty term and variational rule term, respectively. δ and ψ describe the weight coefficients and depth map range of values between W_{da} and W_{re} respectively, and $\psi\subset R^2$. The formula for W_{da} is given in equation (3):

$$W_{da}=\frac{1}{|E(r)|}\sum_{i=1}^{N}\left|E_r y_i-\varepsilon'\right| \tag{3}$$

where, E_r and $E(r)$ describe the number of key frames of the animation image and the number of image frames in the current animation image sequence that are consistent with the information of E_r, respectively. ε' describes the pixel coordinates corresponding to ε within the animated image E_i and E_r under the condition that the depth value is taken as d, and the formula is as in equation (4):

$$\varepsilon'=\pi^{-1}\left[LR_r^i\pi(\varepsilon,d)\right] \tag{4}$$

where, L and $R_r^i\pi$ describe the internal parameters of the camera and the pixel coordinate point position relationship, respectively.

The W_{re} contains the Huber operator inside, which is calculated as in Eq. (5):

$$W_{re}=f(b)\left\|\nabla d(b)\right\| \tag{5}$$

where $f(b)$, ∇d and b describe the depth pixel gradient weight coefficients, depth map gradient and image plane center coordinates, respectively.

In order to solve W_d accurately, m is used to describe the auxiliary variables to obtain Eq. (6):

$$W_d = \int_{\psi} \left[f(b) \mid \nabla d \mid + \frac{1}{2\theta}(d-m)^2 + \frac{\delta}{\mid E(r) \mid} \sum_{i=0}^{n} \left| E_i(\varepsilon) - E_r(\varepsilon, m) \right| \right] d\varepsilon \tag{6}$$

where θ denotes a constant. Compared with Eq. (2), Eq. (6) is converted into a convex optimization problem after the introduction of m, which can be solved and used as the basis for the construction of multi-visual 3D animation models, and texturing and rendering based on the 3D animation models.

II. B.Brightness interpolation

In computer graphics, a smooth curved surface is often represented discretely by a series of polygons. For example, in order to represent the corner of a polished cube, it can be approximated using seven planar slices. However, if the usual polygonal scanning line algorithm is used to draw this approximation, the resulting figure loses the smoothness of the original surface and becomes polyhedral. This is due to the fact that the normal vectors of all points on each plane slice are the same, and after applying the simple illumination model, the luminosity on the same plane slice will remain the same. However, there are discontinuous normal vector jumps between different plane slices, resulting in discontinuous jumps in the luminance of the object surface represented by multiple plane slices.

In order to solve the problem of drawing surface objects approximated by multiple planar slices, various simple algorithms have been proposed, and Gouraud luminance interpolation and Phong normal vector interpolation are two of the most representative methods.

The Gouraud lightness and darkness treatment takes the lightness of a surface surface as a bilinear interpolation of the lightness of the vertices of polygons that approximate the representation of a polysurface. Assuming that a surface object is represented by a polyhedron, and the normal vectors of each polygon are known, then for each vertex, the average of the normal vectors of the polygons sharing the vertex can be taken as the normal vector of the surface at the vertex, and then the normal vectors can be substituted into the illumination model to calculate the value of the luminance of the surface at the vertex.

The calculation of the normal vector at the vertex A is shown in Fig. 1.

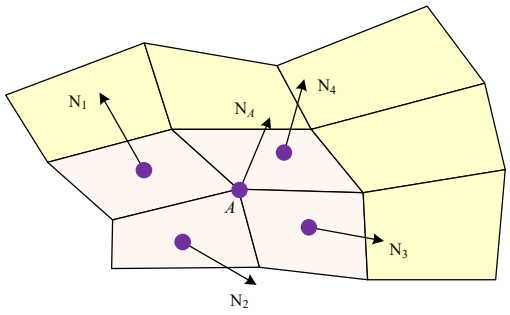

Figure 1: Calculation of the normal vector of vertex A

In Fig. 1, the normal vector of the surface at vertex A can be taken as the average of the unit normal vectors N_1, N_2, N_3, and N_4 of the polygons that share that vertex as in Equation (7):

$$N_A = \frac{1}{4}\left(N_1 + N_2 + N_3 + N_4\right) \tag{7}$$

Before substituting into the lighting model, N_A should be unitized. If the original surface on which the polyhedron is generated is known, and the vertices of the polygon are the sampling points on the original surface, the true normal vector of the original surface at the vertices of the polygon can be taken and directly substituted into the illumination model to calculate the luminance. When the scanning line algorithm is used to draw the above polygons, the luminance at the intersection of the current scanning plane and the boundary of the polygon is first linearly interpolated with the luminance at the vertices of the polygon, and then the luminance at the intersection is linearly interpolated with the luminance at each sampling point on the intersection section of the polygon and the scanning plane. The luminosity of the P point calculated using bilinear interpolation is shown in Figure 2.

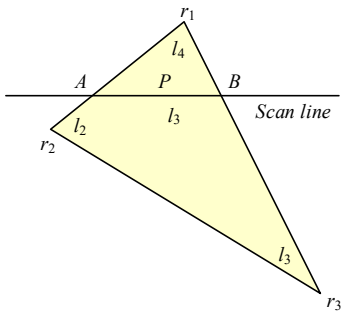

Figure 2: The luminance of point P is calculated by using bilinear difference

Figure 2 shows a scanning plane intersecting a polygon, with the endpoints of the intersection line being the points A and B, and P being a polygon sampling point projected onto the center of a pixel on the corresponding scanning line, with luminosities of the three vertices of the polygon being I_1, I_2, and I_3, respectively. Taking the luminosity I_A of the point A as a linear interpolation of I_1 and I_2, and the luminosity I_B of the point B as a linear interpolation of I_1 and I_3, the luminosity I_P of the point P is a linear interpolation of I_A and I_B. i.e., equations (8)-(10):

$$I_A = uI_1 + (1-u)I_2, \quad u = AV_2 / V_1V_2 \tag{8}$$

$$I_B = vI_1 + (1-v)I_3, \quad v = BV_3 / V_1V_3 \tag{9}$$

$$I_P = tI_A + (1-t)I_B, \quad t = PB / AB \tag{10}$$

where u, v, t are interpolation parameters.

The use of Gouraud brightening not only overcomes the luminosity discontinuity of surfaces represented by polygonal approximations, but is also computationally trivial. In fact, linear interpolation can be computed using the incremental method, where the computational effort involves only one additive computation. As in the above example, the luminosities of all pixels on the AB segment can be computed along the scan line, sequentially from left to right. Let I_A and I_B has been determined, P_1 and P_2 point is adjacent to the coordinates of the two pixels, the difference between the interpolation parameters of the neighboring pixels for Δt, then, it is not difficult to find that the P_2 point luminance I_{P2} and P_1 point luminance I_{P1} has a relationship between the as in equation (11):

$$I_{P2} = I_{P1} + (I_A - I_B)\Delta t = I_{P1} + \Delta I \tag{11}$$

II. C.Production of virtual dynamic interactions

In the virtual three-dimensional environment, three-dimensional interaction technology determines whether the viewer can effectively interact with the virtual object in real time. The specific design and production tools are the application basis for the realization of three-dimensional interactive effects. At present, Virtools software is mainly the mainstream three-dimensional interactive animation production tools, to a certain extent, you can use Virtools software in the virtual interaction function to produce three-dimensional interactive animation form.

Virtools software features and extends the framework mainly includes PhysicsLibrary (physical properties module), AILibrary (artificial intelligence module), VRLibrary (multi-channel immersive display module), Multi-UserServer (network server), 3DOffice/3Dplayer (3D), as well as the support for MAX and 3D display module. Display Module) and output extensions for MAX and Maya, etc., facilitating the creation of interactive animation.

The real interactive dynamic part needs to be imported into Virtools interactive software to complete.

In Maya production part of the main operation and application of the modeling, animation, materials, mapping and other modules, and lighting is not included, Virtools production part of the main application of the Physics Library (Physics Properties Module), the AI Library (Artificial Intelligence Module), the Sharder farm (material rendering), and 3D Office/3D player (3D display). Office/3D player (3D display module) and other common functional modules. The main functions of these modules are: gravity, friction, elasticity, buoyancy and other force fields in the Physics Library, collision detection in the Physics Library, injecting the character with life elements such as thinking and judgment, visual and auditory responses, and tracking, fleeing, hiding, etc. In the AI Library, the character will be able to think, judge, and respond to visual and auditory actions.

III. Optimization and Application of 3D Modeling Technology in Visual Communication

III. A. Algorithm Configuration Experiment

In order to verify the usefulness of the feature extraction and matching (SIFT) algorithm for images, three sets of data are chosen to verify the effectiveness of the algorithm improvement in reducing the amount of operations. Because if the angle between two corresponding images is too large, the feature extraction process will result in too few matches in the matching process due to too few common image regions, the selection of the angle of the images in these three sets of data are smaller to ensure the results of extraction and matching. The angle of these three sets of data are 10, 15 and 30, respectively.Table 1 shows the performance comparison of the algorithm before and after the improvement of the algorithm with different image angle, where “Before” refers to the algorithm before the improvement and “After” refers to the algorithm after the improvement. The performance metrics compared are: (I1) the number of left/right feature points extracted, (I2) the number of total matching pairs, (I3) the number of mis-matched pairs, (I4) the mis-matching rate (%), (I5) the descriptor elapsed time (ms), and (I6) the matching elapsed time (ms).

Table 1: Performance comparison before and after algorithm improvement

Included angle	Algorithm	I1	I2	I3	I4	I5	I6
10°	Before	155/180	44	5	9.31	2011.53	77.90
	After	155/180	41	6	12.51	3565.24	65.22
15°	Before	147/158	36	6	14.29	1999.37	69.37
	After	147/158	31	8	23.34	3499.37	66.36
30°	Before	105/102	18	6	29.42	1478.64	33.69
	After	105/102	16	8	46.67	2963.66	32.64

Analyzing the data in Table 1, it can be learned that the two algorithms have the same number of pairs of feature extraction for images at different pinch angles, and the original algorithm has slightly more than the improved algorithm in terms of the number of (I2) total matching pairs, which is between 0 and 5. With the increase of the image clamp angle, both of them show a decreasing trend in the number of (I2) total matching pairs. In (I4) false matching rate (%), the original SIFT feature extraction algorithm is lower than the improved SIFT algorithm, with a maximum of only 29.42% for the original algorithm. In (I5) descriptor elapsed time (ms), the improved algorithm is higher than the pre-improved algorithm. In terms of (I6) matching elapsed time (ms), the improved algorithm takes less time than the pre-improved elapsed time.

Since both the before and after algorithms have mis-matching in the matching process, the elimination of mis-matching is necessary without strictly restricting the image source and quality, and the RANSAC algorithm is applied to eliminate the errors. And compare the performance of the two algorithms after rejecting the mis-matched pairs is shown in Table 2, where I7 is: total elapsed time (ms).

Table 2: Performance comparison of the two algorithms after eliminating mismatches

Included angle	Algorithm	I1	I2	I3	I4	I7
10°	Before	155/180	41	2	2.51	6063.13
	After	155/180	36	0	0	5523.37
15°	Before	147/158	33	3	6.26	5836.36
	After	147/158	25	2	4.17	5436.86
30°	Before	105/102	17	5	25.01	5000.37
	After	105/102	11	3	20.02	4725.37

From the data in Table 2, it can be seen that the mis-matching rate of the algorithms before and after the improvement has decreased dramatically after error rejection, but the number of errors still tends to increase as the angle increases. In (I7) the overall time consumption (ms), the total time consumption of the improved algorithm is much less, the lowest is only 4725.37 ms. The data set of this paper is a large number of images, and there is no guarantee that randomly matching can be completed between the two images, so the process of error rejection is essential, and at the same time there will be a large number of operations other than feature extraction, and the improved algorithm will save a large amount of time from the rest of the process, and therefore the improved algorithm is in line with the original intention of algorithm improvement.

To sum up the above, this paper chooses the improved SIFT algorithm as the image feature extraction method in the application of digital modeling technology to visual communication design.

III. B. Application testing and analysis

III. B. 1) Efficiency analysis of 3D modeling for corridor bridge space

The eaves, round columns, side windows, beams and accessories of the corridor bridge space are named as sub-models A~sub-model E. They are modeled in 3D using four similar methods (M1, M2, M3, M4) as well as (M5) this paper's method, respectively, and the statistics of the time overhead of modeling for each method is shown in Fig. 3.

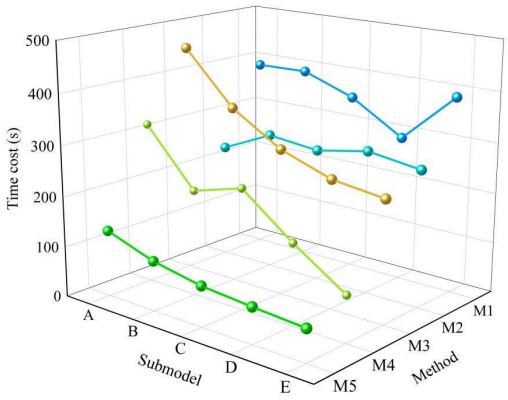

Figure 3: The time cost of 3D modeling of covered Bridges

Figure 3 folding trend shows that in the process of constructing the 3D model of the corridor bridge, the starting time overhead of the (M3) method is too large, and the shortest time used is also as high as 275 s. The time overhead of the (M4) method shows a tendency of decreasing, then increasing, and then decreasing, and the data integrity is poor. Insufficient data in the modeling process reduces the efficiency of 3D modeling. The overall time overhead of the (M2) method is relatively smooth, but the time overhead is greater than 200s on different sub-models, which is less efficient. The (M1) method is similar to the (M4) method, with poor data integrity delivery. In contrast, (M5) method in this paper has the best modeling effect, even if it is necessary to implement the fusion of 3D scanning data and inclined photography data, it does not take too much time, and the time spent on each modeling is about 89-131s, which achieves a better modeling efficiency.

III. B. 2) System Non-Functional Module Testing

In order to further verify the non-functionality of the designed method, the method of this paper is added to the VRay cloud rendering system. The rendering timeliness of VRay cloud rendering is tested, and the rendering performance of the plug-in version of the VRay engine is compared and analyzed with the rendering effect of VRay cloud rendering, and the final rendering results are shown in Table 3. The evaluation items of the selected rendering results are (F1) number of models (pcs), (F2) number of lights (pcs), (F3) number of rendering servers (pcs), the comparison items are (V1) VRay plug-in rendering time (s), (V2) VRay cloud rendering time (s), and the rendering files are (G1) bookcases, (G2) dining table, (G3) dining chairs, (G4) sofa, (G5) curtains, (G6) house plan 1, (G7) house plan 2.

Table 3: Comparison of the rendering results of the two rendering engines

Number	Document	F1	F2	F3	V1	V2
1	G1	6	3	3	57	32
2	G2	8	4	2	54	43
3	G3	5	5	3	40	28
4	G4	4	6	3	42	34
5	G5	8	3	4	57	39
6	G6	31	10	5	501	263
7	G7	42	9	6	489	275

In order to visualize the timeliness of the rendering of the two VRay versions, Table 3 was statistically analyzed and the corresponding rendering time comparisons were plotted in Figure 4.

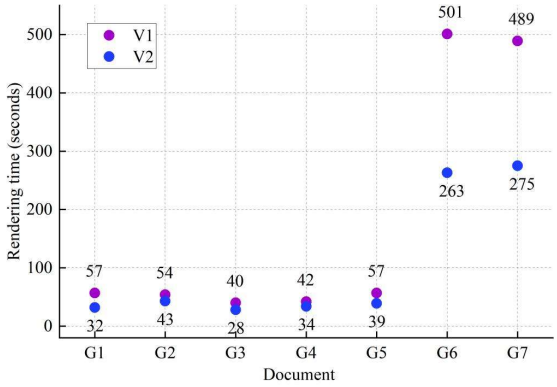

Figure 4: A comparison of the timeliness of rendering between two VRay versions

From the analysis of the above charts, it can be seen that the rendering time of VRay Cloud Rendering is about 45% lower than that of the VRay Engine Plug-in version, the rendering time is significantly lower, as low as 32s, and the rendering speed is better than that of the VRay Engine Plug-in version, which has a better rendering performance.

III. B. 3) Testing and optimization of overall performance

The testing and optimization mainly focuses on a comprehensive evaluation of the system's performance, accuracy and user experience. The results of the comparison between the expected data and the test data are shown in Table 4, and the selected test items are (T1) system latency (ms), (T2) animation smoothness (FPS/s), (T3) speech recognition accuracy (%), (T4) character reaction time (ms), and (T5) user satisfaction (%).

Table 4: The comparison result between the expected data and the test data

Test item	Expected value	Test value	Deviation
T1	15.00	18.46	+3.46
T2	60.00	58.33	-1.69
T3	95.00	91.77	-3.23
T4	50.00	52.15	+2.15
T5	90.00	88.48	-1.52

The data comparison shows that the test results are basically close to the expectation, and the gap between the expected and tested values is between [-5,5]. However, there is still room for improvement in some key performance indicators. For the indicators with large deviations, the combination of hardware upgrading and algorithm optimization is used for gradual improvement. At the same time, the system is continuously improved through iterative testing to ensure that the end-user experience reaches the expected goal.

III. B. 4) Dynamic Interactive Display Sensitivity Testing

In order to further prove the dynamic interaction display sensitivity of the research method in this paper, starting from the first interaction behavior of the test object, the reaction time of the interaction display as well as the animation smoothness are calculated as shown in Table 5, i.e., the delay time of the interaction demonstration. The shorter the time, the higher the sensitivity of the dynamic interactive presentation. The average value of the interactive presentation delay time of the research method in this paper is 0.195s, although there is a certain delay, but the delay time is short and within the acceptable range. The average animation smoothness is 84.825FPS/s, which is a good performance. It shows that under the application of the research method in this paper, the sensitivity of the animation interactive demonstration is high, which can bring a better experience to the user.

Table 5: Interactive demonstration delay time

Action number	Delay time (s)	Animation smoothness (frames/s)
Action 1	0.23	90.58
Action 2	0.14	75.17
Action 3	0.38	77.74
Action 4	0.08	88.85
Action 5	0.16	85.13
Action 6	0.18	80.52
Action 7	0.17	88.55
Action 8	0.22	92.06
Average	0.195	84.825

IV. Conclusion

In this paper, by designing a multi-visual 3D animation modeling method, combined with Virtools interactive software and improved SIFT algorithm, the output of 3D interactive animation art is a more successful research attempt in the innovative integration of digital modeling technology and visual communication design.

Compared with similar algorithms, the designed method takes about 89-131s to model multiple items, which is a high modeling efficiency. And it shows high non-functionality in VRay cloud rendering system, and the rendering time can be as low as 32s on VRay cloud rendering.Overall use, the difference between the test value and the expected value is in the range of [-5,5], which matches the user better. The average value of interactive demo latency is 0.195s, and the average value of animation smoothness is 84.825FPS/s, which combines both animation sensitivity and presentation effect.

References

[1] Maehle, N., Presi, C., & Kleppe, I. A. (2022). Visual communication in social media marketing. The SAGE handbook of social media marketing, 291-306.

[2] Yang, B. (2021, April). Innovation and development analysis of visual communication design based on digital media art context. In 2021 International Conference on Computer Technology and Media Convergence Design (CTMCD) (pp. 192-195). IEEE.

[3] Bian, J., & Ji, Y. (2021). Research on the teaching of visual communication design based on digital technology. Wireless Communications and Mobile Computing, 2021(1), 8304861.

[4] Guan, X., & Wang, K. (2022). Visual communication design using machine vision and digital media communication technology. Wireless Communications and Mobile Computing, 2022(1), 6235913.

[5] Shan, F., & Wang, Y. (2022). Animation design based on 3D visual communication technology. Scientific Programming, 2022(1), 6461538.

[6] Zheng, J., & Liu, Q. (2021, July). Design of 3D scene visual communication modeling based on virtual reality graphics rendering framework. In Journal of Physics: Conference Series (Vol. 1982, No. 1, p. 012183). IOP Publishing.

[7] Rarenko, L. (2019). Animated 3D graphics as visual brand communication on Ukrainian television. International Journal of Innovative Technologies in Social Science, (4 (16)), 31-36.

[8] Li, Y. (2021, April). Analysis of Visual Communication Packaging Design Based on Interactive Experience. In Journal of Physics: Conference Series (Vol. 1852, No. 2, p. 022074). IOP Publishing.

[9] Huang, W., & Hashim, A. M. (2023). Product Packaging Design Innovation based on Visual Communication in Digital Perspective. Revista Ibérica de Sistemas e Tecnologias de Informação, (E62), 468-477.

[10] Wang, F., & Chen, H. (2022). Visual communication method of graphic language in industrial product design. International Journal of Product Development, 26(1-4), 1-11.

[11] Wang, Y. (2022). Product design difference perception model based on visual communication technology. International Journal of Product Development, 26(1-4), 64-76.

[12] Gu, Y., Wang, Q., & Gu, W. (2023). The innovative application of visual communication design in modern art design. Electronics, 12(5), 1150.

[13] Liu, C., Ren, Z., & Liu, S. (2021). Using design and graphic design with color research in AI visual media to convey. Journal of Sensors, 2021(1), 8153783.

[14] Fan, M., & Li, Y. (2020). The application of computer graphics processing in visual communication design. Journal of Intelligent & Fuzzy Systems, 39(4), 5183-5191.